Full Length Article

Improving the processability of coke water slurries for entrained flow gasification

Leon Jampolski [a,*], Alexander Sänger [b], Tobias Jakobs [b], Gisela Guthausen [c], Thomas Kolb [b], Norbert Willenbacher [a]

[a] Karlsruhe Institute of Technology, Institute of Mechanical Process Engineering and Mechanics, Applied Mechanics, 76131 Karlsruhe, Germany
[b] Karlsruhe Institute of Technology, Institute for Technical Chemistry, Gasification Technology, 76344 Eggenstein-Leopoldshafen, Germany
[c] Karlsruhe Institute of Technology, Pro² NMR Institute of Mechanical Process Engineering and Mechanics and Institute of Biological Interfaces 4, 76131 Karlsruhe, Germany

HIGHLIGHTS

- New stabilization concept for coke water slurries based on capillary suspensions.
- Tunability of slurry viscosity in the low shear region while the viscosity in the shear rate range relevant for atomization remains unchanged.
- Visual inspection, centrifugation experiments and magnetic resonance imaging (MRI) reveal strong sedimentation stability.
- Decreased droplet size (SMD) at low GLR during twin-fluid atomization for stabilized slurries provides increased cold gas efficiency.
- Spray angle reduction at low GLR with increasing secondary fluid content may allow for reduced dimensions of the gasification reactor.

GRAPHICAL ABSTRACT
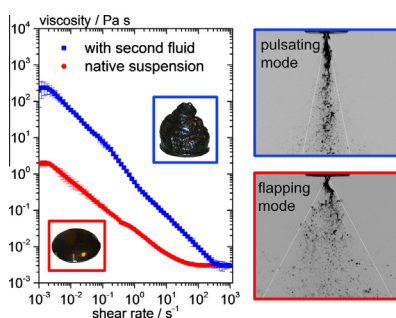
ABSTRACT

A new stabilization concept for coke water slurries based on the capillary suspension phenomenon (Koos and Willenbacher, 2011) is presented. Adding a small amount of an immiscible, secondary fluid to the slurry results in the formation of a sample-spanning particle network controlled by capillary forces. This is accompanied by a strong increase in low shear viscosity controlling sedimentation, whereas the viscosity at high shear rates, relevant for twin-fluid atomization, remains unchanged. Wheat straw and beech wood coke, from fast pyrolysis, suspended in water (mass fraction $\phi_m = 20\%$) have been used as model systems and octanol-1 was added as secondary fluid ($\phi_{sf} = 0$–3.1 vol.%) to proof this concept. Visual inspection, centrifugation experiments as well as nuclear magnetic resonance imaging confirm the drastically increased sedimentation stability offering new opportunities for storage and transport of such slurries.

Atomization of the stabilized slurries was investigated using an external mixing atomizer varying gas-to-liquid ratio (GLR) between 0.5 and 1.5 at a constant liquid mass flow of 10 kg h^{-1}. Sauter mean diameter (SMD) of the created droplets decreases substantially with increasing secondary fluid content, especially at low GLR. SMD reduction is more pronounced for wheat straw than for beech wood coke slurries.

* Corresponding author.
  E-mail address: leon.jampolski@kit.edu (L. Jampolski).

These findings are attributed to the reduction of surface tension induced by the added octanol. Furthermore, the spray angle decreases with increasing octanol content at low GLR. The reported results provide valuable insight for suitable design of the gasification process.

1. Introduction

Biomass is the only renewable carbon source and is supposed to become a major raw material for organic chemistry. Beside this, biomass can be used as fuel in common power plants by torrefaction pretreatment [2], to receive bio-gas (mixture of CH_4 and CO_2) from fermentation [3] or for synthesis gas production (mixture of CO, CO_2, H_2 and H_2O) via gasification [4]. The synthesis gas can subsequently serve as fuel for a gas turbine, e.g. in an IGCC (Integrated Gasification Combined Cycle) to produce heat and power or chemicals through synthesis steps [5]. The bioliq®-process, developed at the Karlsruhe Institute of Technology, provides a new way to use residual biomass (e.g. wheat straw or beech wood). This is done in a two-step procedure. In a first step the biomass is converted by pyrolysis into a high energy density biogenic fluid that is subsequently used as fuel for a high pressure entrained flow gasifier (EFG) [6]. The obtained synthesis gas can be converted by gas cleaning into high value products, such as methanol, liquefied petroleum gas (LPG) or synthetic natural gas (SNG) [7]. Flow behavior of the pyrolysis products is utterly important for almost all process steps. While storage stability (e.g. against sedimentation) is controlled by the viscosity at low shear rates, the intermediate shear rate regime is relevant for unit operations like pumping and mixing, finally the flow behavior at high shear rates is decisive for the atomization in the entrained flow gasifier. Rheology of coal water slurries and its effect on their stability and atomization behavior has been investigated previously. Strong non-Newtonian flow behavior at high particle loading was observed and the dependency of viscosity on particle volume fraction for different types of coal was described [8].

Mansour and Chigier showed experimentally that spray quality is mostly determined by the high shear limiting value of the apparent viscosity [9]. Working with an internal mixing twin-fluid jet atomizer Tsai and Vu confirmed that slurry viscosity has a strong impact on airblast atomization quality but also emphasize the relevance of particle size distribution [10]. Zhao et al. investigated break-up regimes and jet break-up length in highly viscous coal water slurries. Rayleigh type break-up is dominant for these systems and jet break-up length as well as droplet size increase with increasing viscosity [11]. Furthermore, slurry viscoelasticity can also have an impact on the spray structures. Shear wave structure is common for low viscoelasticity while jet oscillation is predominant for high viscoelasticity and additionally the occurrence of periodic spray structures depending on slurry viscosity is reported [12]. Atomization at increased reactor pressure was also examined using an external mixing twin-fluid atomizer because most EFG operate at increased ambient pressure to account for the demand of subsequent process steps. At constant aerodynamic We number an increase of droplet size with increasing ambient pressure was observed [13].

Preventing particle sedimentation in coal water slurries generally requires high energy input (e.g. permanent stirring of storage tanks) and accordingly significant operating costs. Turian et al. investigated the sedimentation of coal particles in water regarding particle size and sphericity. They report a delayed settling rate for smaller and non-spherical particles [14]. Particle settling can be reduced increasing the continuous phase viscosity e.g. using polymeric thickeners (e.g. CMC, rhamsan gum or polymethacrylate)

[15,16]. Low molecular weight amphiphilic additives can be used to control the flocculation and network structure of coal water slurries. Tudor et al. discuss how the settling rate, as well as concentration profile and compression strength of the sediment can be controlled changing the coverage of the particle surface with non-ionic surfactant and upon addition of non-adsorbing polymer to the continuous phase [17].

The addition of an immiscible secondary fluid can have a strong impact on the flow behavior of suspensions. Under certain conditions adding the secondary fluid can result in a viscosity reduction [18,19]. In this work a novel stabilization concept for coke water slurries based on the capillary suspension phenomenon [1] is presented. Adding a small amount (∼1–3 vol.%) of a second immiscible fluid to a suspension results in a sample-spanning and stable particle network controlled by capillary forces. This results in a drastic increase in low shear viscosity and pronounced shear thinning. Two different types of capillary suspensions are observed depending on the three-phase wetting angle $\theta_{(S,B)}$ the secondary fluid forms against the particle surface surrounded by the primary or bulk fluid.

In the pendular state the secondary fluid preferentially wets the particles ($\theta_{(S,B)} < 90$) and forms pendular bridges connecting the particles finally resulting in a percolating network. In the so-called capillary state ($\theta_{(S,B)} > 90$) clusters of particles are formed around small droplets of secondary fluid and these clusters are the building blocks of the sample-spanning network [20]. According to this structure formation capillary suspensions are highly resistant to sedimentation and exhibit unique flow properties. Their flow behavior can be easily adjusted to the demands of different manufacturing or application processes in a wide range [21] selecting the appropriate type and amount of secondary fluid.

The capillary suspension concept has been established as a generic formulation platform for a broad range of innovative materials including novel food formulations [1], capillary suspension based foams [22,23] or pastes for printed electronics providing unique shape accuracy and surface uniformity [24]. Capillary suspensions are even used as precursors for highly porous, high mechanical strength membranes [25,26]. The concept has also been used to control structure formation in particle-laden polymer blends [27] or to assemble metals and nanoparticles into novel nanocomposites superstructures [28].

Here we describe the application of the capillary suspension concept to coke water slurries and we thoroughly discuss its impact on flow behavior, sedimentation stability, i.e. storage and transport, as well as atomization in entrained flow gasification.

2. Materials and methods

2.1. Materials

Coke particles from beech wood and wheat straw were used in this study. Equivalent sphere particle size distribution was determined by Fraunhofer diffraction (HELOS H0309, sympatec GmbH, Clausthal-Zellerfeld, Germany) using an ultrasonic wet dispersing unit (QUIXEL, sympatec GmbH) for dispersing the particles in deionized water. Density was determined using a pycnometer after Gay-Lussac (Carl-Roth GmbH, Karlsruhe, Germany). Porosity was measured with mercury intrusion porosimetry (AutoPore IV,

Table 1
Characteristic physico-chemical specifications of investigated coal particles.

	Wheat straw coke	Beech wood coke
Volumetric mean equivalent sphere diameter	20 μm	12 μm
Particle density	1.85 g cm^{-3}	1.53 g cm^{-3}
Particle porosity	73%	57%
Ash content (DIN 51719)	29.2%	4.5%
Carbon content (DIN 51732)	49.5%	78.5%
Higher heating value (DIN 51900)	20 MJ/kg	30 MJ/kg
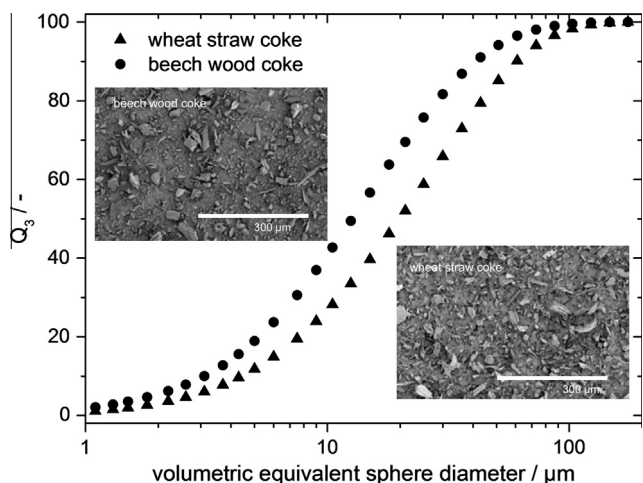
Fig. 1. Volumetric equivalent sphere particle size distributions and SEM images of the investigated wheat straw and beech wood coke particles. Q_3 is the cumulated particle size distribution determined by Fraunhofer diffraction.

micromeritics, Norcross, USA). Furthermore, ash content, carbon content and higher heating value have been determined according to DIN 51719, DIN 51732 and DIN 51900, respectively. Corresponding results are summarized in Table 1, equivalent sphere particle size distributions and respective scanning electron microscopy (SEM) images are shown in Fig. 1.

The SEM images indicate a rough but fairly isometric particle shape with visible pores. The coke was stored under N$_2$ atmosphere in barrels to minimize surface oxidation. Deionized water was used as the bulk phase for the slurries and acted as a model fluid for the aqueous pyrolysis condensate. Octanol-1 (Alfa Aesar, Karlsruhe, Germany) with a density of 0.83 g cm^{-3} and a dynamic viscosity of 9 mPa s was used as secondary phase for the formation of capillary suspensions. Both coke sorts are highly hydrophobic. The three-phase contact angle for beech wood coke in water with added octanol is $\theta_{(S,B)} = 67 \pm 6°$ and for the wheat straw coke with the same conditions it is $\theta_{(S,B)} = 64 \pm 12°$, i.e. both coke types have similar wetting behavior and both systems are supposed to form pendular state capillary suspensions when octanol is added to the aqueous coal slurry.

2.2. Sample preparation

The coke particles were slowly mixed into the bulk fluid using a turbulent beater blade until a homogeneous, air bubble free slurry was achieved. An increase of the angular mixing speed from 400 to 1000 rpm during an additional stirring period of 20 min was performed after all particles had been added to the sample to break remaining agglomerates. Then the secondary fluid was added to the suspension and thoroughly mixed again using a dispensing stirrer at ~1000 rpm for 10 min. This procedure worked for the

lab scale samples with a volume of ca. 50 ml and also for the bigger volume of 40 l needed for the atomization experiments. All rheological measurements were performed right after sample preparation unless otherwise stated.

2.3. Rheological characterization

The rheological properties of the basic fluids and coke water slurries were characterized through the shear rate dependent viscosity (η) as well as the storage (G') and loss (G'') modulus as a function of the angular velocity (ω). Measurements were performed using a rotational rheometer (Physica MCR501, Anton Paar GmbH, Graz, Austria) with a plate-plate geometry (diameter 50 mm, gap height 1 mm) for the lower shear rates ($\dot{\gamma} < 1$ s^{-1}) and a coaxial cylinder geometry (inner diameter 26.66 mm, outer diameter 28.92 mm) for higher shear rates ($\dot{\gamma} > 1$ s^{-1}). Those measurements were conducted using a shear rate ramp (initial shear rate 0.001 s^{-1}, final shear rate 1000 s^{-1}), holding the shear rate for 30 s before recording the shear stress and calculating the corresponding viscosity. Oscillatory measurements were performed using a coaxial cylinder geometry as described above. Frequency sweeps were done at a constant stress amplitude $\sigma_0 = 0.5$ Pa. For the capillary suspensions this corresponds to the linear viscoelastic response regime, the pure coke water slurries do not exhibit linear response for $\sigma_0 \geqslant 0.5$ Pa, but lower stress amplitudes did not reveal reasonable modulus data due to a high noise-to-signal ratio. The temperature for all rheological measurements was 20 °C.

2.4. Sedimentation stability

The sedimentation stability was examined by filling graduated measuring glass cylinders of 500 ml volume with stabilized and non-stabilized slurries at a temperature of 20 °C. After waiting times of several days those filled glass cylinders were investigated optically. A supernatant formed when the coke particles sedimented. To prevent evaporation or other environmental influences these containers were sealed on top. For evaluation of the optical tests each time 20 g of the freshly prepared slurries were put into a centrifuge (Universal 320, Hettich GmbH, Tuttlingen, Germany) at 800 rpm for 6 min. After centrifugation the supernatant of those slurries was scaled and compared to the original mass value. All measurements were performed at least four times.

Magnetic resonance imaging (MRI) experiments were performed on a 200 MHz tomograph (Bruker Avance 200 SWB, Bruker BioSpin GmbH, Rheinstetten, Germany). The superconducting magnet with a 150 mm vertical bore has a magnetic-flux density B_0 of 4.7 T. The Bruker gradient system micro2.5 was used with a ^{1}H NMR linear bird-cage (10 mm inner diameter). The 90° radiofrequency block pulse was 7.5 μs at 0 dB. A sinc-pulse of 1 ms excited the magnetization (30 dB attenuation). For refocusing, a bandwidth matched sinc-pulse of 0.749 ms (21 dB attenuation) was applied. From the pool of imaging pulse sequences provided by Bruker within Paravision® 4.0 (Bruker BioSpin GmbH), the "Rapid Acquisition with Relaxation Enhancement" (RARE) sequence was selected due to the good signal to noise ratio for the chosen experimental time period and the transverse relaxation differences in the sample. Gradient echo sequences were shown not to provide suitable image quality due to the samples specific magnetic susceptibility differences. The cylindrical sample tubes were placed into the sample holder with the symmetry axis along $B_0 \| z$. The measured axial slices with a slice thickness of 0.5 mm ($n = 27$) and an interslice center distance of 0.7 mm were orientated in the xy-plane and measured from bottom to top, while the sagittal slices were oriented in the yz-plane. Data was processed within ParaVision® 4.0 and via self-written scripts in Mat-
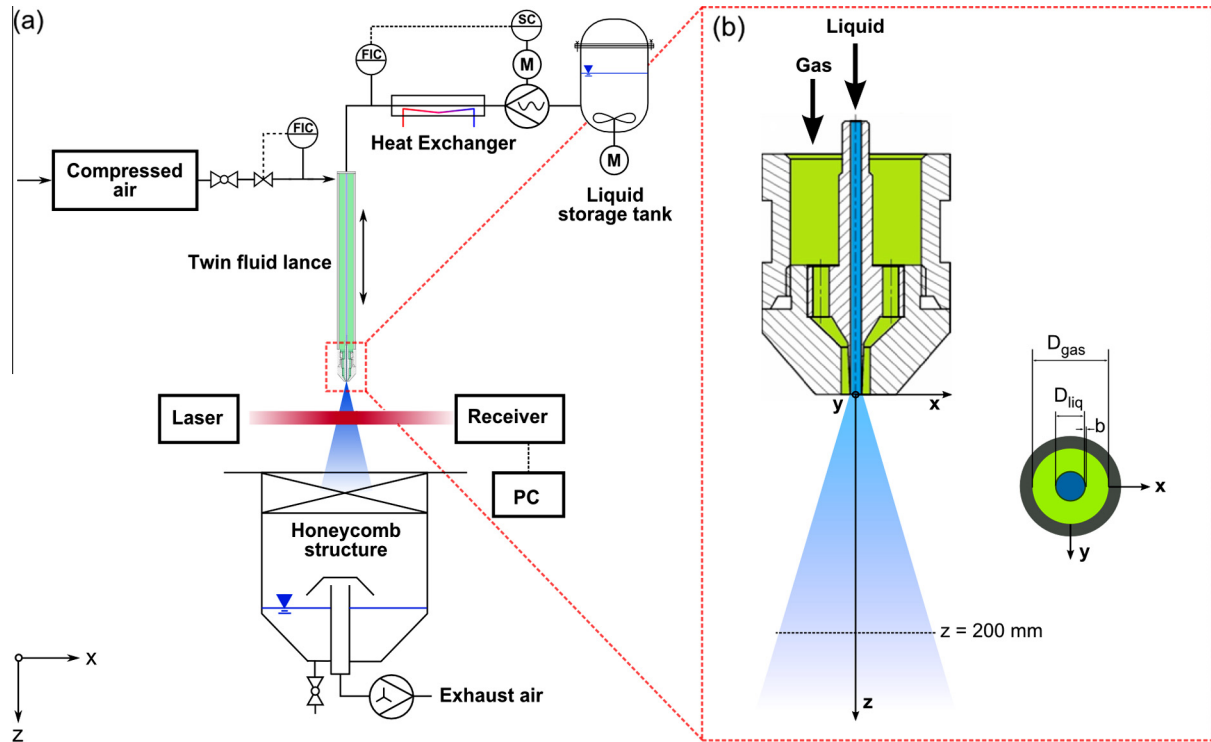
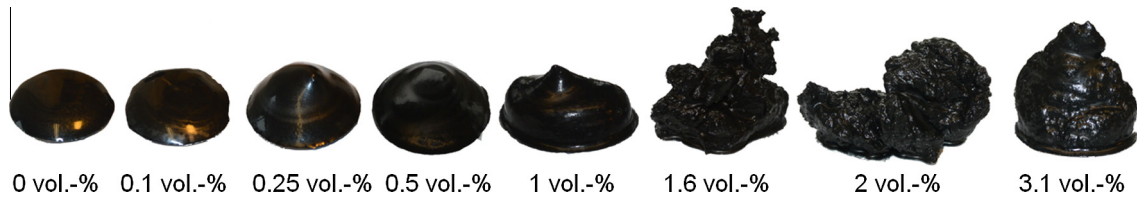Fig. 2. (a) Schematic set-up of the ATMO with (b) the used external mixing twin-fluid nozzle [29].

Fig. 3. Characteristic texture of beech wood coke slurries with increasing content of octanol as second fluid (ϕ_{sf}).

lab® (version R2012a, The MathWorks Inc., Natick, Massachusetts, USA).

2.5. Atomization

Atomization experiments were performed at the atmospheric test rig (ATMO) applying an external mixing twin-fluid atomizer as described in [29]. For a better understanding of the atomization process a simple nozzle geometry (air and liquid are parallel discharged in axial direction) was chosen. The liquid mass flow can be controlled almost pulsation-free in a range of 5–50 kg h^{-1} with an eccentric screw pump (Nemo, Netzsch GmbH, Waldkraiburg, Germany) and is measured by an inductive flow meter (Proline Promass 83A, Endress+Hauser AG, Reinach, Swiss). The air mass flow can be varied between 1 and 20 kg h^{-1} and was measured with hot-wire anemometry (F-206AI, Bronkhorst GmbH, Kamen, Germany). The Sauter mean diameter (SMD) of the droplets was obtained with a Malvern Spraytec drop size detector (Malvern Instruments Ltd., Worcestershire, United Kingdom) mounted 200 mm below the nozzle, as also shown in Fig. 2(b). This device is equipped with a He-Ne-laser with a wavelength of 632.8 nm and a beam diameter of 10 mm. Based on laser diffraction spectroscopy an integral volumetric drop size distribution is measured in the intersection volume of the spray cone and the laser beam line. An evaluation of the measured data was made with the

Mie-theory [30]. The schematic set-up of ATMO is shown in Fig. 2(a) with a more detailed sketch of the twin-fluid nozzle in Fig. 2(b). A high speed camera Photron Fastcam SA-Z (Photron Ltd., Buckinghamshire, United Kingdom) was mounted at two different positions, in the near nozzle region and 200 mm away from the nozzle to proof the sphericity of the droplets, since the Mie-theory is only feasible for round droplets [31]. Further information about the setup can be found in [29]. All measurements were performed at an ambient temperature of 20 °C. The fluid temperature was set to 20 °C using a double pipe heat exchanger.

3. Results and discussion

3.1. Rheological characterization

As shown in Fig. 3 the structure of the beech wood coke slurry changes significantly with increasing secondary fluid content. Suspensions without and with a very small amount (0 vol.% and 0.1 vol.%) of octanol spread as expected for low viscosity suspensions. Further addition of secondary fluid (0.25 vol.% and 0.5 vol.%) results in a more paste-like texture and flow behavior due to a sample spanning network induced by capillary bridges between the particles. With further addition of secondary fluid the slurry becomes stiffer resulting in an improved sedimentation stability, as will be shown later. Fig. 4 shows the viscosity as a function of
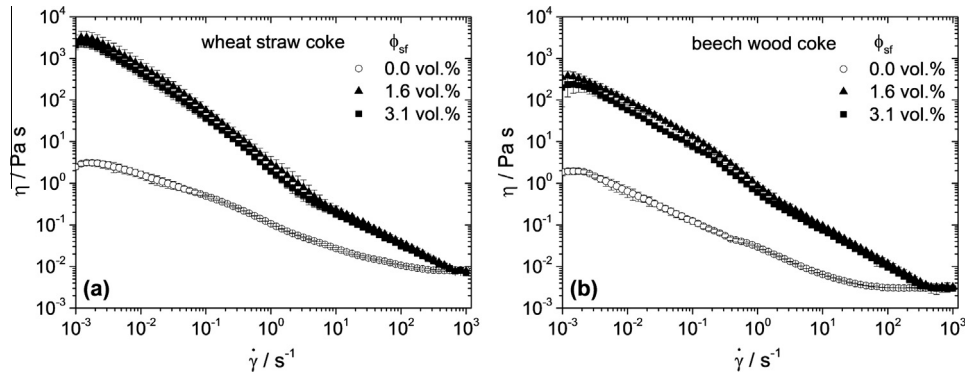
Fig. 4. Viscosity vs. shear rate for slurries of (a) wheat straw coke (ϕ_m = 20%, ϕ_V = 44%) and (b) beech wood coke (ϕ_m = 20%, ϕ_V = 33%).

shear rate for wheat straw coke and beech wood coke slurries at different octanol content. The pure suspensions are shear thinning and both slurries exhibit similar absolute viscosity values at low shear rates, more than three orders of magnitude higher than the viscosity of the continuous phase. This viscosity level is determined by attractive van-der-Waals interactions among particles. A high shear limiting viscosity value is obtained in both cases and according to the higher volumetric particle loading of the wheat straw coke its limiting high shear viscosity is about three times higher than that of the beech wood coke. However, these slurries without a secondary fluid are not stable regarding to sedimentation. Addition of a small amount of octanol changes the flow behavior dramatically. The low shear viscosity increases by orders of magnitude even at an octanol content as low as 1.6 vol.%. In contrast the high shear viscosity is unaffected by the added octanol. The viscosity curves for the pure and capillary suspensions superimpose for $\dot{\gamma}$ > 300 s^{-1}. Obviously, high shear forces destroy the capillary network and it cannot contribute to the viscosity at high shear rates. Similar results have been obtained for other capillary suspension systems [21,24].

The dependence of the low shear viscosity (here measured at $\dot{\gamma}$ = 0.01 s^{-1}) on secondary fluid content is displayed in Fig. 5(a) for both types of coke slurry. For both systems η increases drastically with increasing secondary fluid content and a plateau of the viscosity is reached at $\phi_{sf} \approx 1.5\%$. The absolute value of this plateau is higher for the wheat straw coke slurry than for the beech wood coke system and this is attributed to the higher volumetric particle volume fraction of the former system.

The dramatic change of suspension structure and flow behavior is also directly visible from the shear modulus data shown in Fig. 5 (b). For the pure suspension modulus values are low, G'' increases

linearly with angular frequency and G' is immeasurably small typical for fluid-like systems. However, the suspension including octanol exhibits orders of magnitude higher G', G'' values, G' is essentially independent of frequency and much larger than G'' characteristic for gel-like systems. Data shown in Fig. 5(b) are for wheat straw coke suspensions but similar results confirming the formation of capillary suspensions have been obtained for the beech wood coke slurry, too.

3.2. Sedimentation stability

Samples with 20 wt.% coke were prepared which resulted in ϕ_V = 44% for the wheat straw coke and ϕ_V = 33% for the beech wood coke slurry. After sample preparation the fresh slurry appeared homogeneous as shown in Fig. 6(a). However, particles in the slurry with 0 vol.% octanol settled within a few hours but the supernatant remained strongly opaque, after 8 days the supernatant got transparent as shown in Fig. 6(b). In contrast the slurry with an octanol content of 3.1 vol.% remained as manufactured even after 8 days storage (Fig. 6(c)). This result of visual inspection was further confirmed by centrifugation experiments, applying a relative centrifugal force (RCF) of 71. The dimensionless RCF is given as a multiple of the acceleration of gravity.

$$RCF = \frac{4\pi^2}{g} r n^2 \tag{1}$$

Where r is the radius of the rotor, which is 99 mm for our setup, g is the constant of gravitation and n are the revolutions per second. This allows a comparison of stabilized and non-stabilized slurries within minutes.
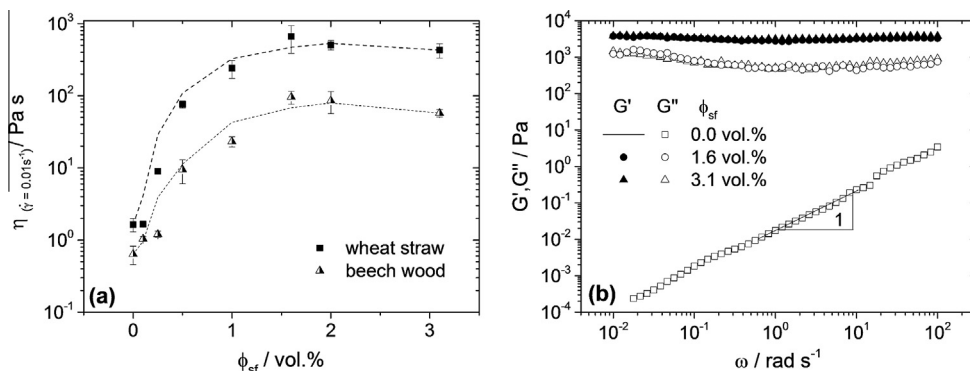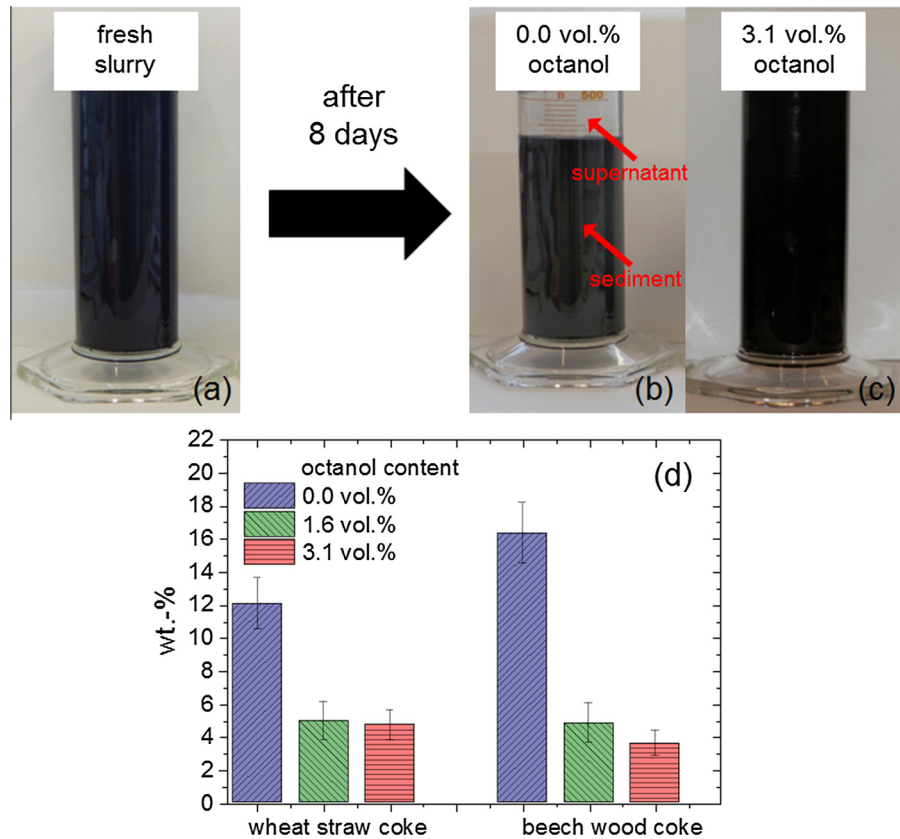

Fig. 5. (a) Low shear viscosity for slurries of beech wood coke and wheat straw coke, both with 20 wt.% particles, at $\dot{\gamma}$ = 0.01 s^{-1} as function of the second fluid volume. (b) Storage (G') and loss (G'') modulus vs. angular velocity ω for a wheat straw coke slurry with ϕ_m = 20% at an octanol content of 0 vol.% and 3.1 vol.%, respectively.

Fig. 6. Beech wood coke slurry (a) freshly prepared and after a storage time of 8 days with (b) an octanol amount of 0 vol.% and (c) 3.1 vol.%, (d) shows supernatant weight relative to the total sample mass of wheat straw and beech wood coke suspensions with ϕ_m = 20 % for octanol contents of 0 vol.% (blue), 1.6 vol.% (green) and 3.1 vol.% (red) after centrifugation for 6 min at 800 rpm.

After procuring this RCF for 6 min the supernatant of the slurries was weighted. The results of those measurements are illustrated in Fig. 6(d). For the wheat straw suspension with 0 vol.% octanol the supernatant weight was ~12% referred to the total sample mass after that procedure and ~16% for the beech wood suspension with 0 vol.% octanol. With an octanol content of 1.6 vol.% for the stabilized suspensions the supernatant content was reduced to about 5% after centrifugation for both slurries. No further reduction of supernatant weight was achieved for the slurries including 3.1 vol.% octanol as expected since the slurries with 1.6 and 3.1 vol.% of secondary fluid exhibit similar low shear viscosity (shown in Fig. 4). The samples are in a low shear viscosity stable plateau. These results clearly demonstrate an increased slurry stability due to the added secondary fluid. This phenomenon was further investigated using magnetic resonance imaging (MRI).

Stable and non-stable slurries were screened by MRI, corresponding images are shown in Fig. 7. The normalized signal intensity is color-coded displayed by the color bar, blue indicates low intensity (close to noise level), which corresponds to the solid material in the sample tube, highlighted by the white lines. Higher signal intensity is represented by colors according to the color bar on the right of each image and indicates the presence of water. A homogenous distribution of coke particles in the sample tubes for the slurries of wheat straw and beech wood with 3.1 vol.% octanol is directly visible in these NMR images. In contrast the samples without a secondary fluid show a pronounced settling of the coke particles for both coke types. Scans in the cross section (axial slice) were also performed confirming the above results. No water could be detected at the tube bottom, as shown in Fig. 7(c), for the samples with 0 vol.% octanol due to the high amount of the settled coke particles. The samples with 3.1 vol.% octanol show a homogenous

mixture of a coke water slurry, indicating that capillary bridges between the particles are present and stabilize the sample. No change in composition was found in the cross section scans for the upper part, as indicated in Fig. 7(b), of the samples containing 3.1 vol.% octanol, while only water was detected in the upper part for the slurries with 0 vol.% octanol. Those results are in agreement with the results of the oscillatory measurements as shown in Fig. 5(b). While the viscous properties predominate for the slurries without octanol, the elastic properties are dominant for those with added octanol.

This improved static stability is required for storage and transportation of coke water slurries as intended in the bioliq®-process and is achieved without further mechanical homogenization treatment. The unique homogeneity of the slurries is also a great benefit for gasification.

3.3. Atomization

The wheat straw and beech wood coke slurries with particle mass fraction of 20% and octanol content of 0, 1.6 and 3.1 vol.% were atomized. The gas-liquid ratio (GLR = $\dot{m}_{gas}/\dot{m}_{liquid}$) was varied according to the values 0.50, 0.75, 1.00 and 1.50 while the liquid mass flow was kept constant at 10 kg h^{-1}. In Fig. 8 the integral Sauter mean diameter (SMD) data detected at 200 mm distance from the nozzle exit are shown as a function of GLR. For measurements without secondary fluid the wheat straw coke slurry has larger SMD than the beech wood coke slurry, since the same mass fraction corresponds to a higher volume fraction and hence higher viscosity of the wheat straw coke slurry. This phenomenon has already been ascertained by Rizkalla and Lefebvre [32]. For increasing GLR both slurries show a strong decrease in droplet size due to
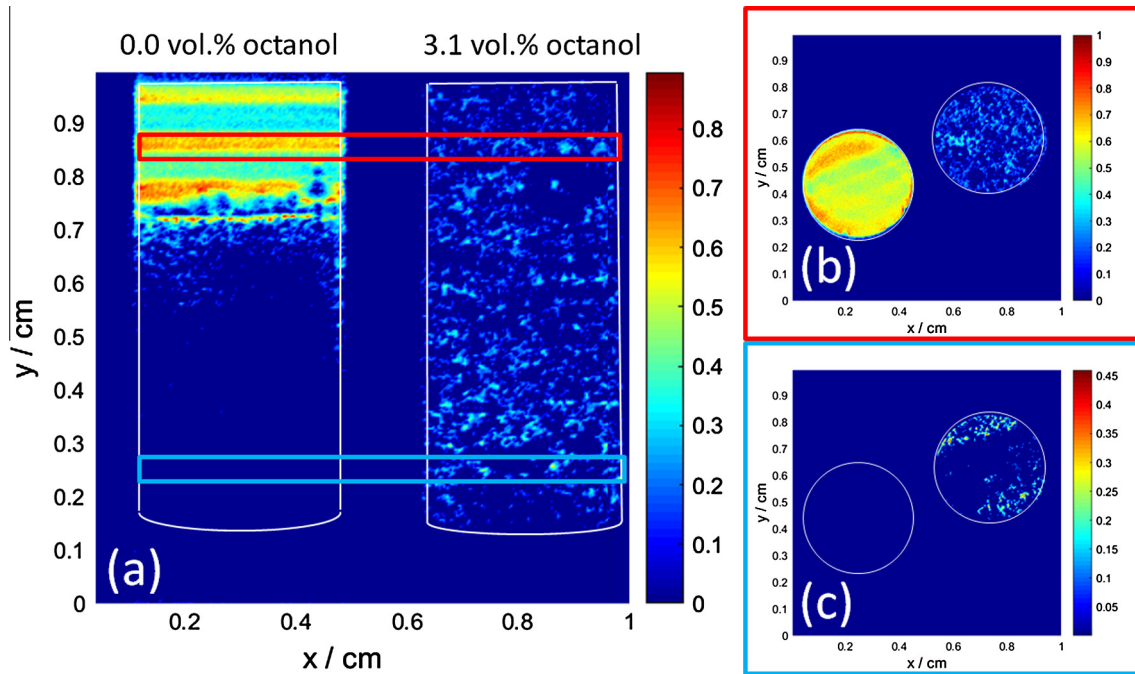
Fig. 7. (a) MRI sagittal images of a wheat straw coke with $\phi_m = 20\%$ and an octanol content of 0 vol.% (left side) and 3.1 vol.% (right side). Additionally, axial slices are shown, which are measured at (b) top and (c) bottom of the samples. The positions are indicated by the rectangles in (a).
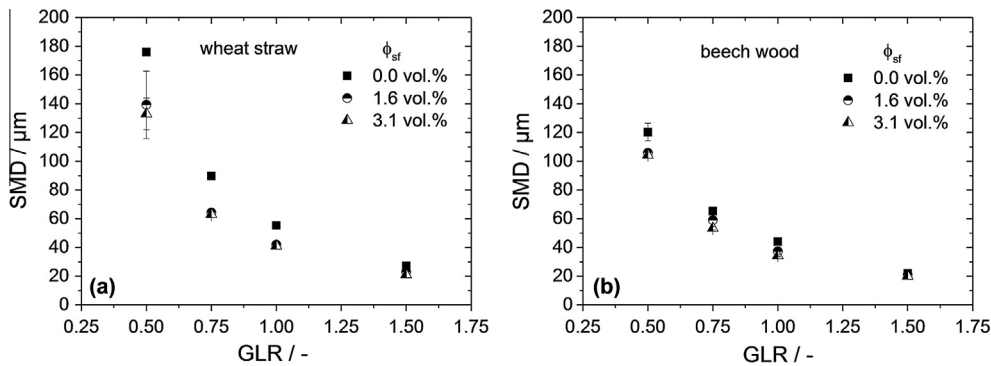
Fig. 8. Integral SMD vs. GLR for (a) wheat straw coke ($\phi_m = 20\%$, $\phi_V = 44\%$) and (b) beech wood coke ($\phi_m = 20\%$, $\phi_V = 33\%$) slurry with increasing octanol content ϕ_{sf}.

the increasing energy input and at a GLR of 1.50 a SMD around 20 μm is found for both slurries.

Beyond that, adding octanol as a secondary fluid results in a SMD reduction, especially at low GLR. At an octanol content of 1.6 vol.% and a GLR of 0.5 the SMD is reduced by 12% (from 120 μm to 106 μm) for the beech wood coke slurry and by 20% (from 176 μm to 139 μm) for the wheat straw coke slurry. Only a minor decrease of the SMD is observed with a further increase of secondary fluid fraction to 3.1 vol.%. In this case beech wood coke slurry exhibit a SMD reduction of 2% (from 106 μm to 104 μm) and the wheat straw coke slurry of 4% (139–133 μm) compared to the suspension with 1.6 vol.%. The effect of secondary fluid on the SMD decreases with increasing GLR and no significant reduction is found for GLR 1.50.

The results suggest that atomization can be performed at a lower energy input when octanol is added to the slurry thus increasing the efficiency of the process. When oxygen is used as gasification agent and atomization agent at the same time, GLR is directly proportional to the stoichiometric ratio applied in an entrained flow gasifier [29]. The necessary mean droplet size could be achieved with lower GLR, which increases the synthesis gas quality (i.e. cold gas efficiency). The trace amount of octanol is not supposed to have a detrimental effect on the quality of the resulting synthesis gas.

As proposed by Mansour and Chigier [9], the atomized fluids, using gas-assisted nozzles, are subjected to high shear rates ($\dot{\gamma} > 1000\ \mathrm{s}^{-1}$). Therefore, the observed reduction in SMD is probably not a viscosity controlled phenomenon since the added secondary fluid does not affect the viscosity at $\dot{\gamma} > 300\ \mathrm{s}^{-1}$. The physical explanation for the observed phenomenon could be the change in surface tension induced by the added secondary fluid. The SMD obtained in a spraying process is related to the dimensionless Weber number (Eq. 2), which describes the ratio of aerodynamic forces to surface tension forces. Depending on definition of L_C, the Weber number (We_i) describes jet break-up ($i = aero$, $L_C = D_{liq}$) or single droplet disintegration ($i = dr$, $L_C = D_{dr}$), where D_{liq} defines the diameter of the undisturbed liquid jet and D_{dr} the diameter of a single drop. Further v_{rel} defines the relative velocity between gas v_{gas} and liquid phase v_{liq}, ρ_{gas} the density of the gas and Γ is the surface tension of the atomized liquid.

$$We_i = \frac{v_{rel}^2 \rho_{gas} L_C}{\Gamma} \qquad (2)$$

Table 2
Surface tension values of wheat straw and beech wood coke slurries at different octanol contents.

Octanol content (vol.%)	Wheat straw (mN m^{-1})	Beech wood (mN m^{-1})
0	72.0 ± 0.6	71.7 ± 0.7
1.6	26.1 ± 4.5	35.4 ± 1.1
3.1	27.6 ± 3.7	34.6 ± 1.3

The higher the Weber number the finer the SMD should be [33]. In this equation the numerator remains constant and only the surface tension may vary upon addition of octanol. Surface tension Γ of the systems investigated here was measured using the pendant drop method [34] and corresponding data are shown in Table 2. In agreement with the results of Rizkalla and Lefebvre [32], the addition of octanol to aqueous coke suspensions decreases the surface tension substantially and thus induces the observed SMD reduction. The more distinctive SMD reduction observed for the wheat straw coke than for the beech wood coke slurries is in line with the higher decrease in surface tension found for the former system. The minor decrease of the SMD with increasing secondary fluid content (1.6–3.1 vol.%) can be attributed to the nearly constant surface tension value of those slurries.

Besides drop size distribution, the spray angle $\overline{\alpha}_{sp}$ was investigated as another important parameter which affects the entrained flow gasification process. Spray angle particularly influences local stoichiometry (ratio of fuel to gasification agent O_2) and probably determines flame expansion in the reactor. From a matrix of

high-speed images the influence of GLR and amount of secondary fluid (ϕ_{sf}) on time averaged spray angle $\overline{\alpha}_{sp}$ can be seen qualitatively. In Fig. 9 the jet disintegration of beech wood coke slurry without and with ϕ_{sf} = 3.1 vol.% secondary fluid octanol is shown for two different gas-to-liquid ratios GLR = 0.5 and 1.5. The gas-to-liquid ratio increases from left to right and the amount of octanol increases from up to down. Comparing Fig. 9(a) with (c) reveals a significant decrease of $\overline{\alpha}_{sp}$ with increasing amount of octanol at low GLR of 0.5. Certainly, this decrease of spray angle can be referred to two different mainly observed primary instabilities of the liquid jet in the near nozzle region. In case of 0 vol.% octanol, as shown in Fig. 9(a), jet disintegration originates predominantly from a primary so-called flapping instability. This phenomenon, which was intensively investigated by Matas and Cartellier [35], is characterized as a non-axisymmetric oscillatory instability. In contrast, the pulsating instability which can be seen in Fig. 9(c) is characterized by the formation of longitudinal waves at the interface between gas and liquid. As investigated and proposed by several authors (e.g. [36,37]), this instability can be classified as a shear induced phenomenon analogous to Kelvin-Helmholtz instability. Consequently, in case of the flapping instability, the ligaments and droplets disintegrating from the intact liquid jet are hurled to left and right, resulting in a large spray angle. In contrast the pulsating instability results in smaller trajectory angles of the droplets that shear off the liquid jet. The reason for this change in primary instability from flapping to pulsating by adding octanol as secondary may be rationalized as follows: As shown by Sänger
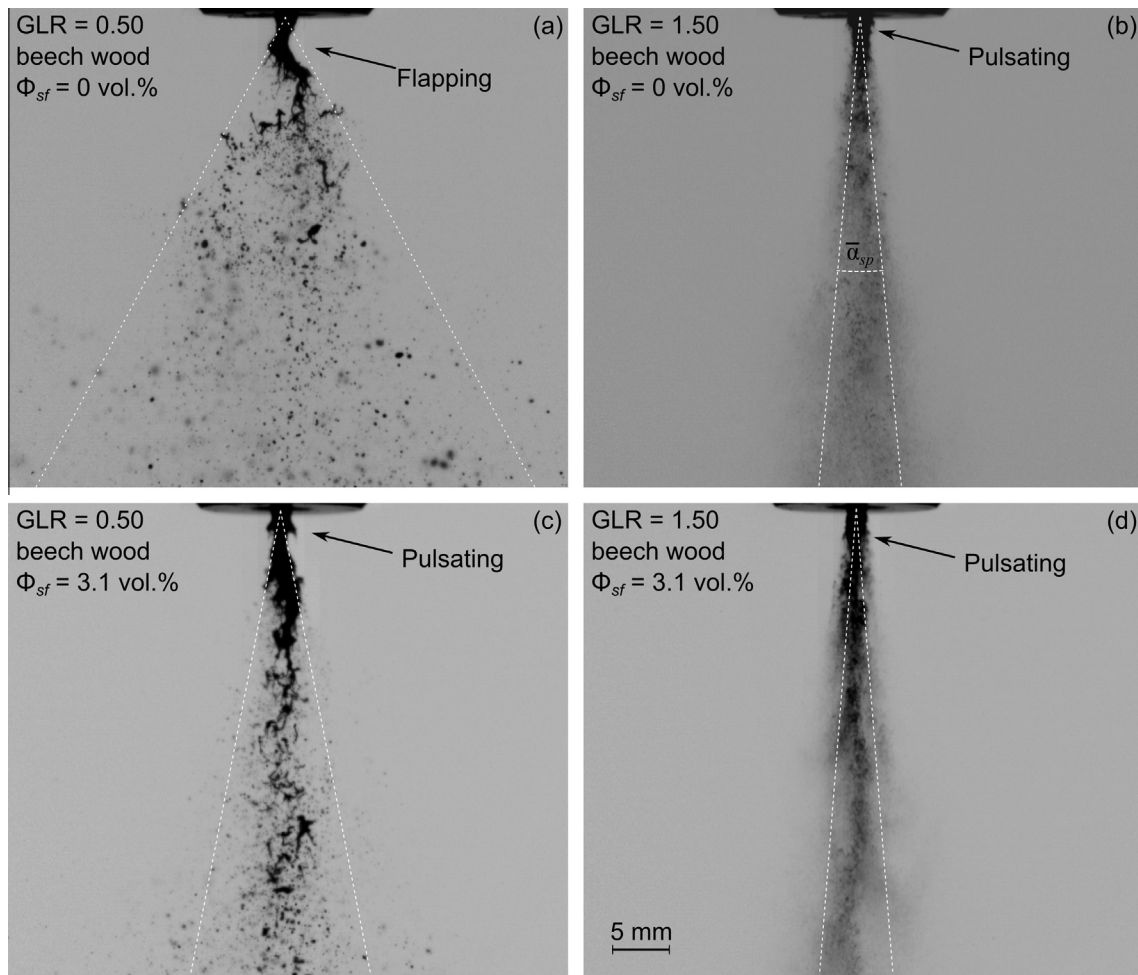
Fig. 9. High-speed visualization of beech wood coke slurry with different amounts of secondary fluid at two different GLR (0.5 and 1.5). The white dashed lines indicate the spray angle $\overline{\alpha}_{sp}$ determined using a threshold value Th$_{sp}$ = 0.9, as explained in the text.

et al. [29] the occurring primary instability (flapping or pulsating) depends on both aerodynamic forces and dynamic viscosity. Atomization of Newtonian liquids covering a wide range of dynamic viscosities using an external mixing twin-fluid atomizer revealed that for low GLR a decrease of liquid viscosity results in a transition from flapping to pulsating mode. Since both liquid viscosity and surface tension stabilize the liquid jet it is assumed, that decreasing surface tension has the same influence as lowering the liquid viscosity. Amplitude height and wave length of the occurring flapping instability decrease with increasing amount of secondary fluid until the dominating flapping instability transforms into mainly occurring pulsating mode. The stabilizing effect of surface tension is reduced with decreasing surface tension as confirmed by measuring the frequency of the occurring primary instability using proper orthogonal decomposition technique [38]. As known from literature [39] increase of destabilizing aerodynamic forces result in increased instability frequency. Therefore a decrease of surface tension should result in an increase in primary instability frequency at constant aerodynamic forces as well. Accordingly, for GLR of 0.5 our analysis revealed that primary instability frequency increases from $f_{prim} = 616\,s^{-1}$ at $71.7\,mN\,m^{-1}$ ($\phi_{sf} = 0$ vol.%) to $f_{prim} = 938\,s^{-1}$ at $35.4\,mN\,m^{-1}$ ($\phi_{sf} = 3.1$ vol.%).

At high GLR the spray angle remains almost constant (see Fig. 9 (b) and (d)) since the pulsating mode is already reached here in both cases (0 and 3.1 vol.% octanol). This is in accordance with a previous study [29] revealing that pulsating instability dominates at high aerodynamic forces. In addition to the influence of octanol, the influence of pure aerodynamic forces can be observed from high-speed images as well. In both cases, $\phi_{sf} = 0$ vol.% (see Fig. 9 (a) and (b)) and $\phi_{sf} = 3.1$ vol.% (see Fig. 9(c) and (d)), an increase of GLR results in decrease of spray angle $\overline{\alpha}_{sp}$.

In addition to the qualitative results presented above, the spray angle $\overline{\alpha}_{sp}$ was determined quantitatively using a set of high-speed images. Time series of images were analyzed using an in-house Matlab® Code (SprayCat). The different steps of the spray angle detection procedure are described in the following: The first step consists in image pre-processing. Homogenization of the slightly inhomogeneous illuminated raw image background was performed using a reference image taken prior to the recording of images with spray. This step enhances image segmentation (see Fig. 10(a)).

To separate the liquid (liquid jet, ligaments and droplets) from the image background each spray image was converted into a binary image (BW image) using the threshold detection algorithm for image segmentation proposed by Kapur et al. [40]. The value 1 (white) belongs to background and 0 (black) to the fluid. For each
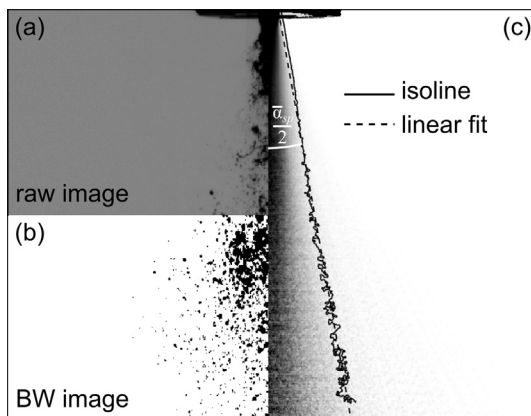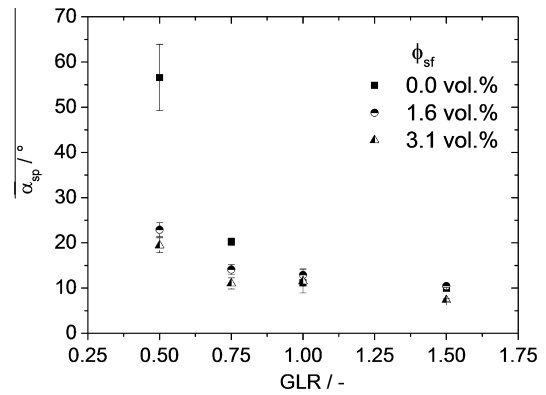
Fig. 11. Spray angle $\overline{\alpha}_{sp}$ of beech wood coke slurry for varying GLR at different secondary fluid volume content ϕ_{sf}.

image this threshold was determined individually to account for possible time dependent variation of image illumination (see Fig. 10(b)). Within a next step all binary images for a given set were superimposed to get a matrix containing information about the successive positions of jet and spray. Dividing each element of this matrix by the number of images given for one set (N_{pic}) results in a matrix containing values between 0 and 1. These values describe the time-integrated probability of finding fluid at a given position (pixel) within the image. When a cell is always filled with fluid the value of this element is 0 and it is 1 when the fluid never passes a given cell. This enables the definition of contour lines with constant values (isoline). Using the coordinates of the contour line with a fixed threshold value $Th_{sp} \in [01]$ on both sides of the spray cone, the edge of the spray can be calculated by means of linear interpolation (see Fig. 10(c)). Finally, the spray angle is calculated from the slope m of both lines using trigonometry $\overline{\alpha}_{sp}/2 = \tan^{-1}(m)$.

For each operational point three data sets with each $N_{pic} = 500$ images were analyzed. In all cases the threshold for determination of the time averaged spray edge was set to a constant value of $Th_{sp} = 0.9$.

For beech wood coke slurry the determined values of the time averaged spray angles $\overline{\alpha}_{sp}$ confirm the qualitative observations. As shown in Fig. 11, $\overline{\alpha}_{sp}$ decreases with increasing amount of octanol. This effect is more pronounced for low GLR than for high GLR. In addition, the spray angle decreases systematically with increasing GLR for all considered slurries (0, 1.6 and 3.1 vol.% octanol) which can be reasoned as follows: The atomization air emerging from the nozzle orifice into the ambient air typically propagates as a free jet. Due to large velocity gradients between the high-speed gas jet and the still ambient air (mixing layer) a distinct amount of ambient air $\dot{m}_s$ is drawn into the free jet. The momentum of this gas flow affects the trajectories of the droplets within the two-phase free jet in a manner counteracting the radial momentum of the droplets. Since the mass flow of suction air is linear proportional to the mass flow directly at the nozzle exit $\dot{m}_{gas}$ [41], we assume that an increase in GLR results in higher momentum and therefore in a decreasing propagation angle of the droplets within the two-phase free jet.

Finally, it should be noted that a similar decrease in spray angle with increasing amount of secondary fluid as well as increasing GLR was also found for the wheat straw coke system. However, the dependencies were less pronounced than for the beech wood coke system.

4. Conclusion

In this work we have introduced a new concept to improve sedimentation stability and atomization of coke water slurries used

Fig. 10. Schema for determination of the spray angle $\overline{\alpha}_{sp}$ with (a) the raw image, (b) the binary image and (c) the analyzed image, while the solid line indicates the isoline and the dashed line the corresponding linear fit.

for biomass energy conversion, e.g. in the bioliq®-process. This concept is based on the capillary suspension phenomenon: a small amount of an immiscible, secondary fluid is added to the suspension resulting in the formation of a sample spanning particle network controlled by capillary forces. This transition from a fluid-like state to a gel-structure is accompanied by a strong increase in low shear viscosity controlling sedimentation whereas the high shear viscosity relevant for atomization is unaffected. Aqueous wheat straw and beech wood coke slurries (ϕ_m = 20%) have been used as model systems and octanol-1 was added as secondary fluid (ϕ_{sf} = 0–3.1 vol.%) to demonstrate the concept. Visual inspection, centrifugation experiments as well as magnetic resonance imaging confirm the drastically increased sedimentation stability, even after several days of storage no sedimentation could be detected. This offers new opportunities for storage and transport of such systems, e.g. storage and transport times can be increased, stirring of storage tanks is rendered unnecessary, clogging of pipes and nozzles is avoided, i.e. process down times may be reduced and process efficiency increases. The effect of secondary fluid on atomization was investigated using an external mixing twin-fluid atomizer varying gas-liquid ratio (GLR) between 0.5 and 1.5 at a constant mass liquid flow of 10 kg h^{-1}. Capillary suspensions were firstly prepared at pilot scale level with batch volumes of 40 l to perform these experiments. The utilized secondary fluid does not affect the higher heating value, for the entrained flow gasification in the bioliq®-process but it has a strong impact on the Sauter mean diameter (SMD) of the produced droplets and the resulting spray angle. Both quantities decrease by adding secondary fluid content. Qualitatively, the observed changes in atomization may be attributed to the remarkable reduction in surface tension induced by the added secondary fluid used here. The SMD reduction is stronger for wheat straw coke than for the beech wood coke and especially pronounced at low GLR suggesting that atomization is enabled at lower energy input (i.e. increased cold gas efficiency). The spray angle decrease observed for both systems has to be taken into account by determining the reactor design. The findings suggest that the capillary suspension concept enhances gasification and may lead to higher process variability and efficiency.

Acknowledgement

References

[1] Koos E, Willenbacher N. Capillary forces in suspension rheology. Science (New York, NY) 2011;331:897–900.
[2] Basu P. Biomass gasification, pyrolysis and torrefaction. 2nd ed. London: Elsevier Inc.; 2013.
[3] Wellinger A, Murphy J, Baxter D. The biogas handbook: science, production and applications. Cambridge: Woodhead Publishing Limited; 2013.
[4] Bridgwater AV. Progress in thermochemical biomass conversion. London: Blackwell Science Ltd.; 2001.
[5] Iglesias Gonzalez M, Kraushaar-Czarnetzki B, Schaub G. Process comparison of biomass-to-liquid (BtL) routes FischerTropsch synthesis and methanol to gasoline. Biomass Convers Biorefinery 2011;1:229–43.
[6] Higman C, Burgt MVD. Gasification. 2nd ed. Amsterdam: Elsevier; 2003.
[7] Dahmen N, Henrich E, Dinjus E, Weirich F. The bioliq® bioslurry gasification process for the production of biosynfuels, organic chemicals, and energy. Energy Sustain Soc 2012;2:3.
[8] Turian RM, Attal JF, Sung D-J, Wedgewood LE. Properties and rheology of coal water mixtures using different coals. Fuel 2002;81:2019–33.
[9] Mansour A, Chigier N. Air-blast atomization of non-Newtonian liquids. J Non-Newtonian Fluid Mech 1995;58:161–94.
[10] Tsai SC, Vu T. Atomization of coal-water slurry using twin-fluid jet atomizer. Fuel 1986;66:1596–602.
[11] Zhao H, Liu HF, Xu JL, Li WF, Cheng W. Breakup and atomization of a round coal water slurry jet by an annular air jet. Chem Eng Sci 2012;78:63–74.
[12] Zhao H, Hou YB, Liu HF, Tian XS, Xu JL, Li WF, Liu Y, Wu FY, Zhang J, Lin KF. Influence of rheological properties on air-blast atomization of coal water slurry. J Non-Newtonian Fluid Mech 2014;211:1–15.
[13] Jakobs T, Djordjevic N, Sanger A, Zarzalis N, Kolb T. Influence of reactor pressure on twin-fluid atomization: basic investigations on burner design for high-pressure entrained flow gasifier. Atomization Sprays 2015;25:1081–105.
[14] Turian RM, Hsu F-L, Avramidis KS, Sung D-J, Allendorfer RK. Settling and rheology of suspensions of narrow-sized coal particles. AIChE J 1992;38:969–87.
[15] Dinçer H, Boylu F, Sirkeci AA, Ateok G. The effect of chemicals on the viscosity and stability of coal water slurries. Int J Min Process 2003;70:41–51.
[16] Usui H, Saeki T, Hayashi K, Tamura T. Sedimentation stability and rheology of coal water slurries. Coal Prep 1997;18:201–14.
[17] Tudor PR, Atkinson D, Crawford RJ, Mainwaring DE. The effect of adsorbed and non-adsorbed additives on the stability of coal-water suspensions. Fuel 1996;75:443–52.
[18] Xu M, Liu H, Zhao H, Li W. How to decrease the viscosity of suspension with the second fluid and nanoparticles? Sci Rep 2013;3:3137.
[19] Zhang J, Zhao H, Li W, Xu M, Liu H. Multiple effects of the second fluid on suspension viscosity. Sci Rep 2015;5:16058.
[20] Bossler F, Koos E. Structure of particle networks in capillary suspensions with wetting and nonwetting fluids. Langmuir 2016;32:1489–501.
[21] Koos E, Johannsmeier J, Schwebler L, Willenbacher N. Tuning suspension rheology using capillary forces. Soft Matter 2012;8:6620.
[22] Zhang Y, Wu J, Wang H, Meredith JC, Behrens SH. Stabilization of liquid foams through the synergistic action of particles and an immiscible liquid. Angew Chem – Int Ed 2014;53:13385–9.
[23] Zhang Y, Allen MC, Zhao R, Deheyn DD, Behrens SH, Meredith JC. Capillary foams: stabilization and functionalization of porous liquids and solids. Langmuir 2015;31:2669–76.
[24] Bitsch B, Dittmann J, Schmitt M, Scharfer P, Schabel W, Willenbacher N. A novel slurry concept for the fabrication of lithium-ion battery electrodes with beneficial properties. J Power Sources 2014;265:81–90.
[25] Dittmann J, Koos E, Willenbacher N. Ceramic capillary suspensions: novel processing route for macroporous ceramic materials. J Am Ceram Soc 2013;96:391–7.
[26] Dittmann J, Maurath J, Bitsch B, Willenbacher N. Highly porous materials with unique mechanical properties from smart capillary suspensions. Adv Mater 2016;28:1689–96.
[27] Domenech T, Velankar S. Capillary-driven percolating networks in ternary blends of immiscible polymers and silica particles. Rheol Acta 2014;53:593–605.
[28] Xu J, Chen L, Choi H, Konish H, Li X. Assembly of metals and nanoparticles into novel nanocomposite superstructures. Sci Rep 2013;3:1730.
[29] Sänger A, Jakobs T, Djordjevic N, Kolb T, South KITC. Effect of primary instability of a high viscous liquid jet on the spray quality generated by a twin-fluid atomizer. In: ILASS Europe, 26th annual conference on liquid atomization and spray systems; 2014.
[30] Hergert W, Wriedt T. The Mie theory. Berlin: Springer; 2012.
[31] Pollack JB, Cuzzi JN. Scattering by nonspherical particles of size comparable to a wavelength: a new semi-empirical theory and its application to tropospheric aerosols. J Atmos Sci 1980;37:868–81.
[32] Rizkalla AA, Lefebvre AH. Influence of liquid properties on airblast atomizer spray characteristics. J Eng Power 1975;97:173.
[33] Bayvel L, Orzechowski Z. Liquid atomization. Washington, DC: Taylor & Francis; 1993.
[34] Song B, Springer J. Determination of interfacial tension from the profile of a pendant drop using computer-aided image processing. 2. Experimental. J Colloid Interface Sci 1996;184:77–91.
[35] Matas J-P, Cartellier A. Flapping instability of a liquid jet. C R Méc 2013;341:35–43.
[36] Villermaux E. Mixing and spray formation in coaxial jets. J Propul Power 1998;14:807–11.
[37] Raynal L, Villermaux E, Lasheras J, Hopfinger E. Primary instability in liquid gas shear layers. 11th International symposium on turbulent shear flows 1997;3:271–5.
[38] Arienti M, Soteriou MC. Time-resolved proper orthogonal decomposition of liquid jet dynamics. Phys Fluids 2009;21:1–15.
[39] Lin S. Breakup of liquid sheets and jets. Cambridge: Cambridge University Press; 2003.
[40] Kapur J, Sahoo P, Wong A. A new method for gray-level picture thresholding using the entropy of the histogram. Comput Vis Graph Image Process 1985;29:140.
[41] Günther R. Verbrennung und Feuerung. Berlin: Springer; 1984.